

INVESTIGATING THE INFLUENCE OF CONTROL SYSTEMS OF MULTI-INFEED HVDC SYSTEM ON AC/DC POWER SYSTEM VOLTAGE STABILITY BY MODAL ANALYSIS METHOD

Guohong Wu Tamotsu Minakawa Toshiyuki Hayashi
Tohoku Gakuin University Tohoku Gakuin University Tohoku University
Sendai, Japan

wugh@tjcc.tohoku-gakuin.ac.jp minakawa@tjcc.tohoku-gakuin.ac.jp moden02@ec.ecei.tohoku.ac.jp

Abstract – This paper presents a rigorous method to investigate the influence of control systems of multi-infeed HVDC system on AC/DC power system voltage stability. For this purpose, a continuous power flow computation method, which takes into account power system controls not only the Automatic Voltage Regulator (AVR) and the speed governor (GOV) in power generation but also voltage control systems such as the On-Load Tap Control (OLTC) and the Automatic Control of Shunt Capacitor (ACSC), etc., is proposed in this study. Furthermore, modal analysis method was applied to the voltage stability analysis of multi-infeed HVDC systems to study the mechanism of voltage stability. The computation results from an AC/DC model system with dual HVDC systems verified the efficiency of the proposed method and quantitatively illustrated the influence of control systems of HVDC system and Over Excitation Limiter (OEL) on AC/DC power system voltage stability.

Keywords: *voltage stability, power flow, control system, modal analysis, AC/DC system, multi-infeed HVDC*

1 INTRODUCTION

With the increasingly stressed conditions under which power systems must operate and the occurrence of many power system blackouts due to loss of voltage stability, the ability to maintain voltage stability has become of great concern^{[1][2]}. Especially, when a system suffers a long-term continuous disturbance in the absence of sufficient reactive power support, voltage instability may occur along with some changes in power network conditions such as slowly but continuously increasing loading, facility outage, and voltage or power generation control operations. Since conventional HVDC system absorbs reactive power on both its rectifier and inverter sides, the behavior of HVDC may be a major factor that influences the voltage stability of AC/DC systems^[3]. Furthermore, with the increased use of HVDC systems in power networks, a situation may arise in which two or more HVDC systems feed into AC system locations that are in close proximity electrically, which is called multi-infeed HVDC power system. In this power system, new phenomena resulting from interactions between the various AC and DC systems may occur^[4], and thus investigation and clarification of the voltage stability of these systems is required.

In view of the importance of voltage stability assessment for multi-infeed HVDC power systems, a few researchers have been engaged in its study for several years. In the report by Aik and Andersson [5], an eigenvalue decomposition-technique-based method is used for analyzing the relationship between the voltage stability and some of the HVDC parameters, such as short-circuit ratio and coupling impedance between the constituent AC/DC subsystems. However, to date, few studies aimed at the analysis of the influence of control systems of

multi-infeed HVDC system on voltage stability have been presented. According to our study, a difference in voltage stability may occur depending on control modes of HVDC system following variation of bus voltage on its inverter. Therefore, the objective of the present study was to investigate how the control systems of HVDC system influence the voltage stability of a multi-infeed HVDC system during a long period of system condition changes.

Some important factors are thought to have a great impact on voltage stability and need to be taken into consideration. These include the Automatic Voltage Regulator (AVR) and its Over Excitation Limiter (OEL), the speed governor (GOV) and its Automatic Generation Control (AGC) on the generator side, and On-Load Tap Control (OLTC) for transformers, Automatic Control of Shunt Capacitor (ACSC) and control systems of HVDC system on the network side. Load voltage and frequency characteristics are also big factors for voltage stability. In order to take all of the above-mentioned factors into account when performing long-term voltage stability analysis, the following two technologies are considered to be necessary:

(1) A power flow computation method that can take power system controls into consideration and that can provide a continuous “snapshot” of power system conditions along a time-domain trajectory. This is necessary because some of these controls strongly depend on power system conditions. For example, the GOV adjusts the generator mechanical input by monitoring the deviation in frequency, the AVR controls the generator excitation voltage by monitoring the deviation in generator terminal voltage, while the transformer taps, the amount of ACSC, the active and reactive power of load and HVDC system, the changeover between control modes of HVDC system are determined by bus voltages and system frequency. Long-term domain power flow computation, which can provide information on the variations of bus voltages and system frequency, is therefore necessary. The conventional power flow computation method, in which the frequency is assumed to be constant and generators and loads are treated as PV and PQ nodes, respectively, cannot accomplish this task. For this reason, a new power flow computation method is proposed in this work.

(2) A method of voltage stability analysis that can take power system controls into consideration for assessment of voltage stability for each system condition. The modal analysis method^{[6][7][8]} is adopted and applied to the voltage stability analysis of multi-infeed HVDC systems. The contribution of this work to modal analysis method is that the influence of voltage control systems such as AVR with OEL and controls of HVDC can be investigated simultaneously in our approach.

This article is organized as follows. The power flow computation method herein proposed is presented and demonstrated

by application to an AC/DC model system with dual HVDC systems in section 2. The power flow results given in this section are also used to analyze the voltage stability in the following sections. In section 3, the modal analysis method is briefly explained and its application to the model system is depicted, followed by illustration of the influence of control systems of HVDC system and OEL on voltage stability in section 4. Conclusions are summarized in the last section.

2 POWER FLOW COMPUTATION METHOD CONSIDERING POWER SYSTEM CONTROLS

2.1 Power Flow for One System Condition

With consideration of the control characteristics of GOV, AVR (& OEL), load and HVDC systems, the nonlinear characteristic equation for a balanced AC/DC system in steady-state can be expressed as follows^[9]:

$$\begin{cases} F_1(\delta, V, f) = P_e(\delta, V, f) - P_m(f) = 0 \\ F_2(\delta, V, f) = P_{SL}(\delta, V, f) - P_L(V, f) = 0 \\ G_1(\delta, V, f) = E_f(\delta, V, f) - E_{fd}(V) = 0 \\ G_2(\delta, V, f) = Q_{SL}(\delta, V, f) - Q_L(V, f) = 0 \\ \delta_0 = 0 \end{cases} \quad (1)$$

where $F_1, G_1 \in \mathfrak{R}^m$, $F_2, G_2 \in \mathfrak{R}^n$, $V, \delta \in \mathfrak{R}^{m+n}$, $f, \delta_0 \in \mathfrak{R}^k$. m and n are the total number of generators and loads, k is the total number of AC sub-networks divided by HVDCs, P_e and P_m are vectors of generator power output and its mechanical input, E_{fd} and E_f are vectors of AVR output and excitation voltage seen from the system side, P_L and Q_L are vectors of active and reactive powers absorbed by the load or HVDC systems and, P_{SL} and Q_{SL} are those injected to the load or HVDC nodes from the network, and V, δ and f are vectors of voltage magnitudes, phase angles and frequencies.

Assuming that the reference phase angle δ_0 for each sub-network is zero and invariable, the updates for phase angles, voltage magnitudes and frequencies can then be computed with the same procedure of conventional Newton-Raphson Method using the following linearized equation:

$$[\Delta X] = -[J]^{-1}[\Delta F G] \quad (2)$$

where

$$\begin{aligned} [\Delta X] &= [\Delta \delta \quad \Delta V \quad \Delta f], \\ [\Delta F G] &= [P_e - P_m \quad P_{SL} - P_L \quad E_f - E_{fd} \quad Q_{SL} - Q_L \quad 0], \\ [J] &= \begin{bmatrix} \frac{\partial P_e}{\partial \delta} & \frac{\partial P_e}{\partial V} & \frac{\partial P_e}{\partial f} - \frac{\partial P_m}{\partial f} \\ \frac{\partial P_{SL}}{\partial \delta} & \frac{\partial P_{SL}}{\partial V} - \frac{\partial P_L}{\partial V} & \frac{\partial P_{SL}}{\partial f} - \frac{\partial P_L}{\partial f} \\ \frac{\partial E_f}{\partial \delta} & \frac{\partial E_f}{\partial V} - \frac{\partial E_{fd}}{\partial V} & \frac{\partial E_f}{\partial f} \\ \frac{\partial Q_{SL}}{\partial \delta} & \frac{\partial Q_{SL}}{\partial V} - \frac{\partial Q_L}{\partial V} & \frac{\partial Q_{SL}}{\partial f} - \frac{\partial Q_L}{\partial f} \\ 0 \cdots 1 \cdots 0 & 0 & 0 \end{bmatrix}. \end{aligned}$$

Due to space constraints, the detailed expressions for elements in J are not presented here.

It can be seen that this method has the following features:

(1) With the consideration of characteristics of AVR, GOV and load/HVDC systems, the specification of PV and PQ in the conventional power flow method is replaced by the specification of initial mechanical power input P_{m0} and initial excitation voltage E_{fd0} . The generator output and terminal voltage are determined by GOV and AVR, and the absorbed active and

reactive powers by load/HVDC systems do not remain constant.

(2) The system frequency is treated as a variable and calculated. The swing node, which is necessary in the conventional power flow computation for the balance of active and reactive power in the system, is no longer needed. The active and reactive powers of the system are automatically balanced by GOV, AVR with the generators and loads and HVDCs in the network.

2.2 Power Flow Along Time Domain Trajectory

The computation method in 2.1 provides the power flow condition at one equilibrium point. In this chapter, a method is presented for continuously obtaining system conditions along a time domain trajectory while system is undergoing continuous disturbances such as slowly but continuously increasing loading, various contingencies, facility outage and under voltage or power generation controls. The system controls considered in this study are GOV (& AGC), AVR (& OEL) on the generator side, OLTC for load transformers, ACSC and controls of HVDC on the network side, and the load characteristics are also taken into consideration. The control systems of HVDC include OLTC for converter transformers, an Automatic Power Control (APC) and an Automatic (DC) Current Control (ACC) on its rectifier side, and the changeover between an Automatic (DC) Voltage Control (AVC) and an Automatic extinction advance angle Control (γC) modes on its inverter side.

A computation flow chart is presented in Fig. 1. The time interval can be on the order of seconds, and 2.5 s or 5 s are considered as proper choices. In this work, 2.5 s is used.

It can be seen that, this method computes system conditions continuously by tracing the equilibrium point of the power

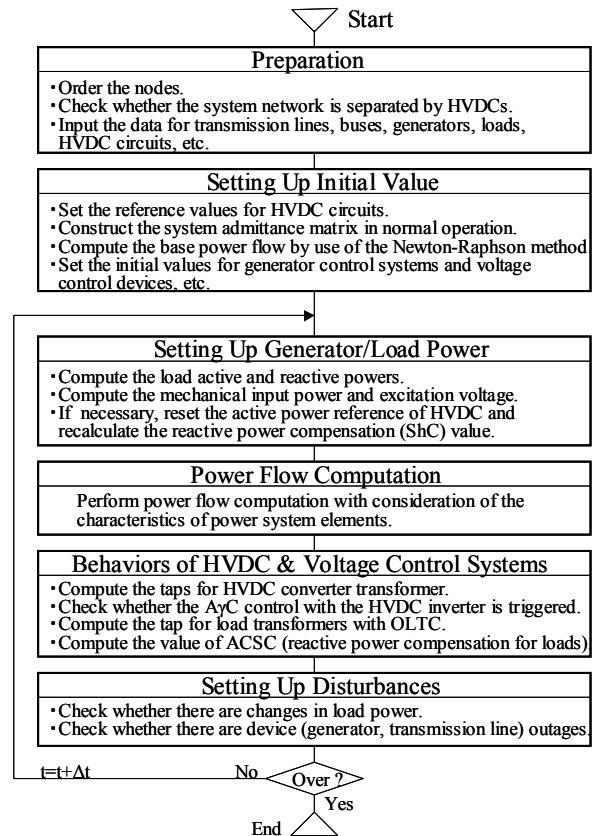


Fig. 1: Flow chart of Continuously Equilibrium Point Tracing Power Flow Computation Method

system along the time domain trajectory. Thus, it is termed “Continuously Equilibrium Point Tracing Power Flow Computation Method” herein.

2.3 Example

The above method is applied to a model system with dual HVDC systems given in Fig. A1 (Appendix B). Block diagrams for system controls are as follows: GOV and AVR for generators are shown in Fig. A2; Control systems for HVDC system are given in Fig. A3, and that for OLTC and ACSC are in Fig. A4 and Fig. A5. The main generator constants are listed in Table A1. The continuous system conditions along the time domain trajectory are computed in the cases listed in Table 1. Disturbance is assumed to be a 25% increase in load PL_1 lasting 7 minutes starting at 1 min. The system condition profiles for case 1 are shown in Fig. 2, and some selected figures for all the three cases are given in Fig. 3. These results are also used for voltage analysis in the following sections.

	Case 1	Case 2	Case 3
$K_{\alpha 2}$	30.0	60.0	30.0
K_{β}	30.0	30.0	60.0

$K_{\alpha 2}$ and K_{β} : Control gains in HVDC systems (Fig. A3)

Table 1 Cases for continuous power flow computation

Figure 2 illustrates the variations in some important state variables of sub-network 1 (inverter side) including the following: generator outputs, frequency, critical bus voltages, operation of OLTC and ACSC, ignition advance angles and operation behavior of $A\gamma C$ with HVDC systems. From these figures, the following can be observed:

- At first, along with the load increase, both G0 and G1 increase their output in an attempt to maintain the system frequency. However, due to the AGC control with G1, the output of G0 (connected to the tie line, see Fig. A1) is gradually restrained from about 2 min.

- The bus voltages first start to decrease, but thanks to the AVR control, the terminal voltage of generator G1 at bus 2 does not drop so much, until the OEL of its AVR actuates at 6.25 min. (point P4) to bring its excitation voltage down. Accompanying the operations of OEL, the bus voltages considerably dip and trigger the swing in the system.

- Since the voltage of HVDC2 inverter terminated bus 9 continues decreasing together with the load increase, the $A\gamma C$ for HVDC2 inverter commences operation at 1.83 min. (point P2) instead of the normal AVC control so as to maintain sufficient extinction advance angle, this operation further aggravates the voltage of bus 9, and the voltage decrease spreads to bus 8 and leads to the $A\gamma C$ operation with the HVDC1 inverter before long (point P3), which brings about further voltage decrease in these buses.

- The voltage decrease of bus 9 directly results in a decrease in the voltage of bus 3. Hence, the OLTC changes the tap of load transformer T_L at 2.125 min. in an attempt to restore the voltage of bus 3, but this operation leads to greater power absorption by the load and further drop in the voltage of bus 9. Even the ACSC increase in a stepwise fashion beginning at 5.75 min. in an attempt to restore the voltage of bus 9, due to its slow operation, the voltage drop of bus 9 continues and finally triggers the operation of OEL with G1, which starts the system swing.

- In the meantime, the ignition advance angles (β) can be observed to decline accompanying the voltage drop of the buses, while HVDC inverters are controlled by AVC. When

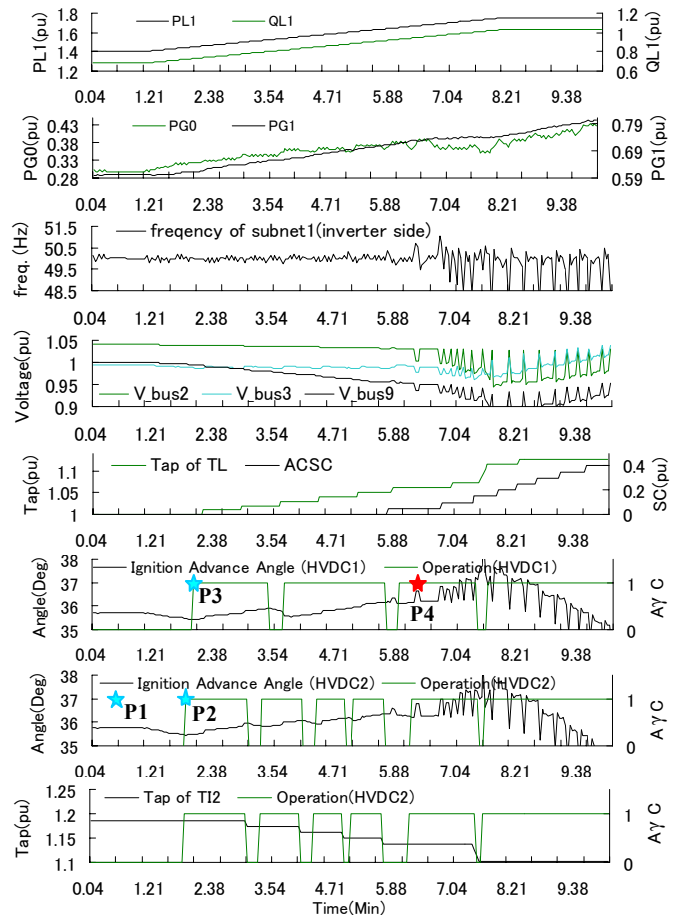


Fig. 2: System condition profiles along the time domain trajectory (case 1)

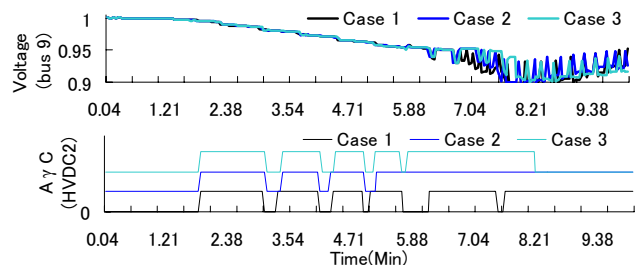


Fig. 3: Selected figures for all three cases

$A\gamma C$ starts to work, however, β again rises, so as to maintain sufficient extinction advance angle γ_0 . A changeover between these two control modes occurs responding to the tap change with the converter transformer at HVDC inverter sides.

Figure 3 shows the influence of control gains with HVDC systems on voltage profiles and HVDC $A\gamma C$ operations. It can be seen that the gains do not greatly affect the voltage profiles, and the operation of the $A\gamma C$ in these cases do not vary so much as well during the period of time when the voltage of inverter terminated bus 9 is larger than 0.95pu. However, when the voltage of bus 9 is lower than 0.95pu, the $A\gamma C$ operation becomes complicated since it is affected by both control systems and tap changer of converter transformer with HVDC systems.

Figure 2 and Fig. 3 can give a general overview of the system voltage stability, but do not provide deeper insight. In practice, we want to know the degree of voltage stability, its change as a consequence of system condition changes, and the

mechanism of voltage instability. For this purpose, a voltage analysis method is necessary and such a method is addressed in the following section.

3 VOLTAGE STABILITY ANALYSIS

3.1 V-Q Modal Analysis

Considering the active and reactive power flow at a node in the power system shown in Fig. 4, equation (3) can be obtained.

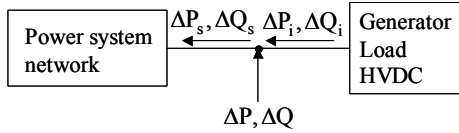


Fig. 4: Power flow at a node in power system

$$\begin{bmatrix} \Delta P \\ \Delta Q \end{bmatrix} = \begin{bmatrix} \Delta P_s \\ \Delta Q_s \end{bmatrix} - \begin{bmatrix} \Delta P_i \\ \Delta Q_i \end{bmatrix} \quad (3)$$

The symbols in equation (3) represent the following:

$\Delta P, \Delta Q \in \mathfrak{R}^{m+n}$: incremental active and reactive power, respectively, injected into the node.

$\Delta P_s, \Delta Q_s \in \mathfrak{R}^{m+n}$: incremental active and reactive power, respectively, absorbed by network, which can be derived by ordinary power flow solution and expressed by

$$\begin{bmatrix} \Delta P_s \\ \Delta Q_s \end{bmatrix} = \begin{bmatrix} \partial P_s / \partial \delta & \partial P_s / \partial V \\ \partial Q_s / \partial \delta & \partial Q_s / \partial V \end{bmatrix} \begin{bmatrix} \Delta \delta \\ \Delta V \end{bmatrix} \quad (4)$$

$\Delta P_i, \Delta Q_i \in \mathfrak{R}^{m+n}$: incremental active and reactive power, respectively, injected from power elements such as the generator, load or HVDC, which can be represented as

$$\begin{bmatrix} \Delta P_i \\ \Delta Q_i \end{bmatrix} = \begin{bmatrix} \partial P_i / \partial \delta & \partial P_i / \partial V \\ \partial Q_i / \partial \delta & \partial Q_i / \partial V \end{bmatrix} \begin{bmatrix} \Delta \delta \\ \Delta V \end{bmatrix} \quad (5)$$

The derivation of expressions (5) can be found in Appendix A.

$\Delta \delta, \Delta V \in \mathfrak{R}^{m+n}$ in (4) and (5) are the incremental voltage angle and magnitude, respectively.

From (3)-(5), the linearized steady-state system power voltage equations can be obtained and written as

$$\begin{bmatrix} \Delta P \\ \Delta Q \end{bmatrix} = \begin{bmatrix} J_{P\delta} & J_{PV} \\ J_{Q\delta} & J_{QV} \end{bmatrix} \begin{bmatrix} \Delta \delta \\ \Delta V \end{bmatrix} \quad (6)$$

System voltage stability is affected by both P and Q. However, when only the incremental relationship between ΔQ and ΔV is desired to evaluate the voltage stability, ΔP can be assumed as zero and the relation of $\Delta \delta = -J_{P\delta}^{-1} \cdot J_{PV} \cdot \Delta V$ can be obtained from (6). Thus, we have

$$\Delta Q = J_R \cdot \Delta V \quad (7)$$

where $J_R = J_{QV} - J_{Q\delta} \cdot J_{P\delta}^{-1} \cdot J_{PV}$.

And then, (7) can be transferred as follows:

$$\begin{aligned} \eta \cdot \Delta V &= \Lambda^{-1} \cdot \eta \cdot \Delta Q \\ \Delta V_k &= \frac{1}{\lambda_k} \cdot \Delta Q_k \end{aligned} \quad (8)$$

where η is the left eigenvector of J_R , Λ is the diagonal matrix of eigenvalues of J_R , and $\Delta V_k, \Delta Q_k$ are the k th elements of $\eta \Delta V$ and $\eta \Delta Q$, respectively.

It is known from (8) that the larger the magnitude of positive $1/\lambda_k$, the closer the k th modal voltage is to being unstable; if $\lambda_k < 0$, the voltage of the system is unstable. Therefore, $1/\lambda_k$ determines the degree of system voltage stability and can be used as an index for it. Therefore, $1/\lambda_k$ is thus called "Voltage Sensitivity Index (VSI)" in this work.

3.2 Example

Modal analysis at the P1 equilibrium point in Fig. 2 is carried out. The largest (critical) two VSIs in case 1 are 0.5142 and 0.1207, which means that the system is voltage stable in this case. For understanding the key contributing factors to these two critical VSIs, their participations with all nodes in sub-network 1 are shown in Fig. 5. All of their participations with nodes in sub-network 2 are almost zero.

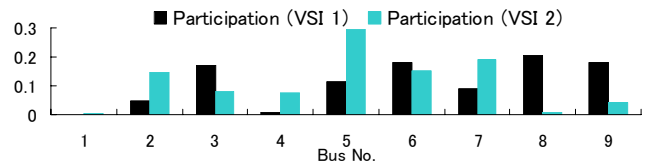


Fig. 5: Participation of VSIs with all buses in the model system

Figure 5 shows that the critical VSIs mainly participate with buses 2, 3, 5, 6, 7, 8 and 9, which are all in sub-network 1. This indicates that sub-network 1 may be potentially prone to voltage stability problems. The participation of these critical VSIs also provides some information on the voltage-weak points and involved areas. As can be seen from Fig. 5, buses 3, 6, 8 and 9, which are in proximity to HVDCs, are the most critical points, and the area connected to HVDC inverters is the one of greatest concern. A reactive compensation measure in this area may therefore lead to the best voltage stability enhancement in this case.

4 VOLTAGE ANALYSIS RESULTS FOR THE MODEL POWER SYSTEM

When system controls commence operation and change the system conditions, voltage stability is greatly different in prior and latter situation. To understand the mechanism of voltage stability well, some special system conditions such as the equilibrium points where the control modes of system is changed need to be given great attention and studied well.

All the equipment mentioned in the first section may affect the voltage stability to some extent. Because of the constraints of this paper, only the influence of control systems of HVDC system and that of OEL are presented herein.

4.1 Influence of Control Gains with HVDC Systems

To investigate the influence of control gains with HVDC systems, modal analysis around the initial operating point (P1 in Fig. 2) and the HVDC2 A γ C control operating point (P2 in Fig. 2) for case 1- case 3 (Table 1) is accomplished and the results of the two most critical VSIs are given in Table 2. These gains are assumed to be primarily determined for other purpose, not for voltage stability.

Note the difference in VSI 1 and VSI 2 between case 1, case 2 and case3. It is seen that the change of control gains in HVDC systems do not bring about tremendous change in

	P1		Before P2		After P2	
	VSI 1	VSI 2	VSI 1	VSI 2	VSI 1	VSI 2
Case 1	0.5142	0.1207	0.5145	0.1231	0.5816	0.1235
Case 2	0.5142	0.1207	0.5100	0.1225	0.5830	0.1237
Case 3	0.5119	0.1207	0.5078	0.1224	0.5815	0.1237

Before P2: HVDC1 (AVC), HVDC2 (AVC);

After P2: HVDC1 (AVC), HVDC2 (A γ C).

Table 2: Results of VSIs around P1 and P2 points

voltage stability, a result that is in agreement with that in section 2. In any case, when the control mode is AVC (P1 & Before P2), larger gains (case 2, case 3) lead to a little better voltage stability than the smaller one (case 1). On the contrary, larger gains with ACC (case 2) may bring to a little worse voltage stability while A γ C is in operation (After P2).

4.2 Influence of HVDC Control Mode

In normal inverter operations, the HVDC is in operation with AVC; however, when the terminal bus voltage is dropped too much, the A γ C is actuated automatically instead of AVC to reserve a sufficient margin angle to avoid commutation failures [10]. To investigate the influence of this changeover between the control modes with the HVDC systems, voltage analysis is conducted around the point where only the HVDC2 A γ C control is operating (P2 in Fig. 2) and the point where both HVDC A γ C controls are operating (P3 in Fig. 2). The results with control parameters set as per case 1 to case 3 are given in Table 3.

		Before P2	After P2	Before P3	After P3
		Case 1	VSI 1	0.5145	0.5816
	VSI 2	0.1231	0.1235	0.1234	0.1240
Case 2	VSI 1	0.5100	0.5830	0.5796	0.6894
	VSI 2	0.1225	0.1237	0.1233	0.1239
Case 3	VSI 1	0.5078	0.5815	0.5782	0.6898
	VSI 2	0.1224	0.1237	0.1233	0.1239

Before P2: HVDC1 (AVC), HVDC2 (AVC);

After P2: HVDC1 (AVC), HVDC2 (A γ C);

Before P3: HVDC1 (AVC), HVDC2 (A γ C);

After P3: HVDC1 (A γ C), HVDC2 (A γ C).

Table 3: Results of VSIs around P2 and P3 points

From Table 3, it can be seen that when the control mode changes from AVC to A γ C, the VSIs especially the most critical one, i.e., VSI 1 considerably skips, which is a warning that although A γ C can help to avoid commutation failures, aggravation of voltage stability is sacrificed. In order to keep voltage stable in AC/DC power systems, we must take notice to the worst voltage stability case such as the point "After P3", not only for normal operating conditions such as point P1. In some cases, a compensation measure, i.e., a new voltage control algorithm or some var compensation, may be needed to prevent a system from facing voltage instability accompanying some changes in operating conditions.

4.3 Influence of OEL

Figure 2 shows that, the operation of OEL is a very important factor that is responsible for the swing in the system. The influence of OEL is thus briefly discussed here, although it may be thought to be beyond the concept of this paper. The voltage stability result around the first time OEL operating point (P4 in Fig. 2) in case 1 is as follow:

Before OEL operation: VSL 1: 0.9138; VSL 2: 0.1556

After OEL operation: VSL 1: 1.1218; VSL 2: 0.2174

It is seen that both VSI 1 and VSI 2 considerably skip following the operation of OEL. When the system later experiences such OEL operation several times as can be observed in Fig. 2, it gradually tends to be unstable. These results verify the prediction that OEL operation may damage the voltage stability of power systems.

5 CONCLUSION

The influence of control systems of multi-infeed HVDC system on AC/DC power system voltage stability was investigated in this work by performing continuous power flow tracing and modal analysis. The results from a power system model with dual HVDC systems revealed the following facts:

- When system conditions is changed following some disturbances in an AC/DC power system, control systems such as AGC, OLTC, ACSC, OEL and HVDC A γ C control might be automatically brought into operation. Some of these controls are expected helpful for voltage stability; however, when control mode of HVDC systems is changed from AVC to A γ C and when OEL commences operation following the drops of bus voltage, it has been confirmed that the voltage stability can be considerably aggravated. The results forthcoming from this study also remind us that it is necessary to take notice to the worst voltage stability case in an AC/DC power system, not only for normal operating conditions.

- The change of control gains in HVDC systems do not greatly affect the system voltage stability, but, a larger gain may have a positive effect while HVDC inverter side is controlled by AVC and may also have an opposite influence while A γ C is actuated. Also, the change in control gains does not bringing about notable changes in the system condition profiles along the time domain trajectory.

The contributions of this study are as follows:

- (1) A continuous power flow computation method has been presented that can take the power system controls into consideration. These control systems include AVR and its OEL, GOV and its AGC with the generators, and OLTC, ACSC, load characteristic and HVDC controls in the network. The proposed method is especially useful for investigating the long duration phenomena in power systems.

- (2) An approach to the voltage stability analysis of multi-infeed HVDC systems has been made by use of the modal analysis method. Formularization for modal analysis considering the AVR with OEL and HVDC control systems has been fulfilled and described in this work.

REFERENCES

- [1] C. Canizares, et al., "Voltage Stability Assessment: Concepts, Practices and Tools", IEEE/PES Power System Stability Subcommittee Special Publication, August 2002
- [2] CW. Taylor, "Power System Voltage Stability", EPRI Power System Engineering Series, McGraw-Hill, Inc., 1994
- [3] A.E. Hammad, W. Kuhn, "A Computation Algorithm for Assessing Voltage Stability at AC/DC Interconnections", IEEE trans. on Power Systems, Vol. PWR-1, No. 1, pp. 209~215, February 1986
- [4] J. Reeve, S.P. Lane-Smith, "Multi-infeed HVDC Transient Response and Recovery Strategy", IEEE trans. on Power Delivery, Vol. 8, No. 4, pp. 1995~2001, October 1993
- [5] Denis Lee Hau Aik, G. Andersson, "Voltage Stability Analysis of Multi-infeed HVDC Systems", IEEE trans. on Power Delivery, Vol. 12, No. 3, pp. 1309~1316, July 1997

- [6] P. Kundur, "Power System Stability and Control", EPRI Power System Engineering Series, McGraw-Hill, Inc., 1994
- [7] B. Gao, G.K. Morison, P. Kundur, "Voltage Stability Evaluation Using Modal Analysis", IEEE trans. on Power Systems, Vol. 8, No. 1, pp. 1529-1542, November 1992
- [8] P-A Lof, G. Andersson, D.J. Hill, "Voltage Stability Indices for Stressed Power Systems", IEEE trans. on Power Systems, Vol. 7, No. 4, pp. 326-335, February 1996
- [9] T. Nagao, N. Uchida, "Load Flow Calculation with Generator & Load Characteristics", CRIEPI Reports, No. 180008, 1980 (in Japanese)
- [10] S. Sato, K. Yamaji, et al., "Development of a Hybrid Margin Angle Controller for HVDC Continuous Operation", IEEE trans. on Power Systems, Vol. 11, No. 4, pp. 56-62, November 1996

APPENDIX A

The derivation of Equation (5) is described in this appendix. Due to space constrains, only an outline of the derivation of the HVDC linearized equation is presented here. Models for obtaining the linearized equations of generator and loads are given as well. The detailed concepts of these equations will be presented in other papers.

A.1 Linearized Equation of HVDC

The power absorbed by HVDC can be expressed as

$$\begin{cases} P_{di} = 0.67524 \cdot V_i \cdot I_d \cdot [\cos(\alpha_i + \mu) + \cos \alpha_i] / n_i \\ Q_{di} = 0.67524 \cdot V_i \cdot I_d \cdot [\sin(\alpha_i + \mu) + \sin \alpha_i] / n_i \\ P_{dj} = -0.67524 \cdot V_j \cdot I_d \cdot [\cos \beta_j + \cos(\beta_j - \mu)] / n_j \\ Q_{dj} = 0.67524 \cdot V_j \cdot I_d \cdot [\sin \beta_j + \sin(\beta_j - \mu)] / n_j \end{cases} \quad (A-1)$$

where

$P_{di}, Q_{di}, P_{dj}, Q_{dj}$: active and reactive power absorbed by HVDC rectifier and inverter, respectively;

V_i, V_j : voltage magnitude of HVDC rectifier and inverter connected bus, respectively;

I_d : DC current;

α_i, μ, β_j : ignition delay angle for rectifier, overlap angle and ignition advance angle for inverter, respectively; and

n_i, n_j : tap rate of transformer for HVDC rectifier and inverter, respectively.

Linearizing (A-1), we have

$$\begin{cases} \Delta P_{di} = J_{P_{dvi}} \cdot \Delta V_i + J_{P_{did}} \cdot \Delta I_d + J_{P_{dai}} \cdot \Delta \alpha_i \\ \Delta Q_{di} = J_{Q_{dvi}} \cdot \Delta V_i + J_{Q_{did}} \cdot \Delta I_d + J_{Q_{dai}} \cdot \Delta \alpha_i \\ \Delta P_{dj} = J_{P_{dvi}} \cdot \Delta V_j + J_{P_{did}} \cdot \Delta I_d + J_{P_{d\beta j}} \cdot \Delta \beta_j \\ \Delta Q_{dj} = J_{Q_{dvi}} \cdot \Delta V_j + J_{Q_{did}} \cdot \Delta I_d + J_{Q_{d\beta j}} \cdot \Delta \beta_j \end{cases} \quad (A-2)$$

From the HVDC control systems given in Fig. A3, we obtain

$$\begin{bmatrix} \Delta I_d \\ \Delta \alpha_i \\ \Delta \beta_j \end{bmatrix} = \begin{bmatrix} J_{I_{dvi}} & J_{I_{dvj}} \\ J_{\alpha_{ivi}} & J_{\alpha_{ivj}} \\ J_{\beta_{jvi}} & J_{\beta_{jvj}} \end{bmatrix} \cdot \begin{bmatrix} \Delta V_i \\ \Delta V_j \end{bmatrix} \quad (A-3)$$

Apply (A-3) to (A-2), we obtain

$$\begin{bmatrix} \Delta P \\ \Delta Q \end{bmatrix} = \begin{bmatrix} 0 & J_{pv} \\ 0 & J_{qv} \end{bmatrix} \cdot \begin{bmatrix} \Delta \delta \\ \Delta V \end{bmatrix} \quad (A-4)$$

where

$$\Delta P = [\Delta P_{di} \quad \Delta P_{dj}]^T, \Delta Q = [\Delta Q_{di} \quad \Delta Q_{dj}]^T, \text{ and} \\ \Delta \delta = [\Delta \delta_i \quad \Delta \delta_j]^T, \Delta V = [\Delta V_i \quad \Delta V_j]^T.$$

A.2 Generator Model

Generators are represented with an induced voltage behind synchronous impedance model expressed as follows:

$$\begin{bmatrix} V_d \\ V_q \end{bmatrix} = \begin{bmatrix} 0 & f \cdot X_q \\ -f \cdot X_d & 0 \end{bmatrix} \cdot \begin{bmatrix} I_d \\ I_q \end{bmatrix} + \begin{bmatrix} 0 \\ f \end{bmatrix} \cdot E_{fd} \quad (A-5)$$

Generator active and reactive power outputs are computed by

$$\begin{bmatrix} P_g \\ Q_g \end{bmatrix} = \begin{bmatrix} I_d & I_q \\ -I_q & I_d \end{bmatrix} \cdot \begin{bmatrix} V_d \\ V_q \end{bmatrix} \quad (A-6)$$

A.3 Load Models

Two types of load models have been used for the loads in Fig. A1.

Load PL_1 and PL_{101} are with voltage and frequency characteristic given by

$$\begin{aligned} P_L &= P_0 \left(\frac{n_i \cdot V_i}{V_0} \right)^{\alpha_p} \left(1 + \frac{\beta_p}{100} (f - f_0) \right) \\ Q_L &= (Q_0 - P_0) + P_0 \left(\frac{n_i \cdot V_i}{V_0} \right)^{\alpha_q} \left(1 + \frac{\beta_q}{100} (f - f_0) \right) \end{aligned} \quad (A-7)$$

where

V_i, V_0 : voltage magnitude and its rated value of load bus, respectively;

f, f_0 : frequency and its rated value, respectively;

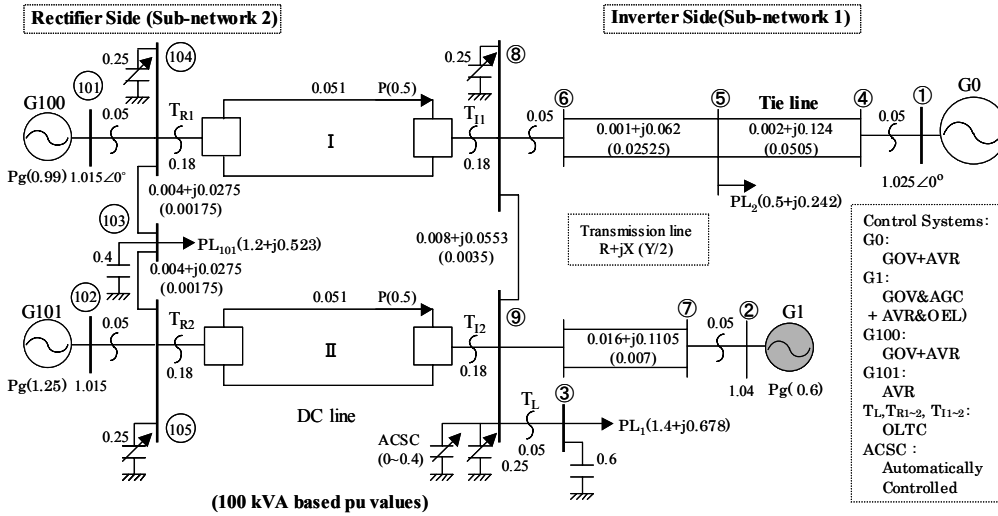
n_i : tap rate of load transformer; and

$\alpha_p, \beta_p, \alpha_q, \beta_q$: coefficients with values of 1.0, 2.0, 2.7 and -2.0, respectively.

Load PL_2 are with voltage characteristic given by

$$\begin{aligned} P_L &= P_0 \left(\frac{V_i}{V_0} \right)^2 \\ Q_L &= Q_0 \left(\frac{V_i}{V_0} \right)^2 \end{aligned} \quad (A-8)$$

APPENDIX B



	G0	G1
MVA	500	100
Xd	1.79	1.864
Xq	1.79	1.864
Xl	0.135	0.3
Rf	0.0011	0.0018
Ra	0.001	0.0021

* Constants of G100 (200MVA) and G101 (200MVA) are the same as that of G1

Table A1: Generator Constants

Fig. A1: Power system model with dual HVDC systems

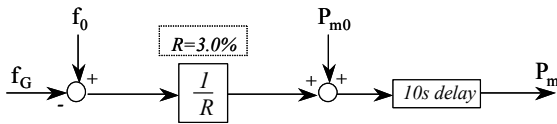


Fig. A2 (a): GOV for G0, G100

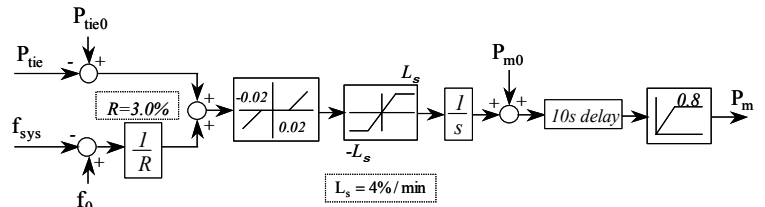


Fig. A2 (b): GOV for G1

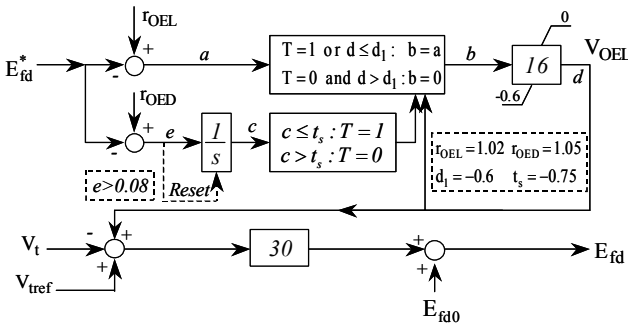


Fig. A2 (c): AVR for G1

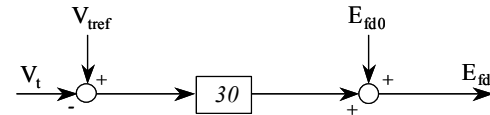


Fig. A2 (d): AVR for G0, G100, G101

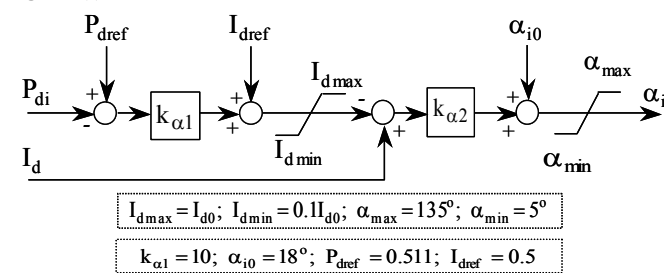


Fig. A3 (a): APC+ACC control with HVDC rectifier side

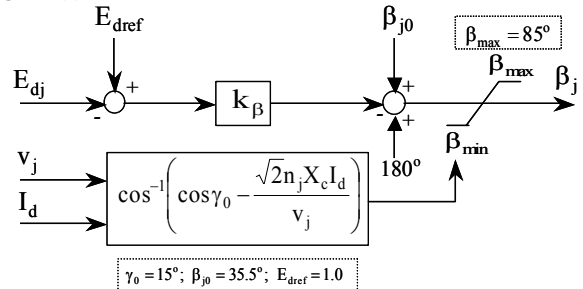


Fig. A3 (b): AVC-A gamma C control with HVDC inverter side

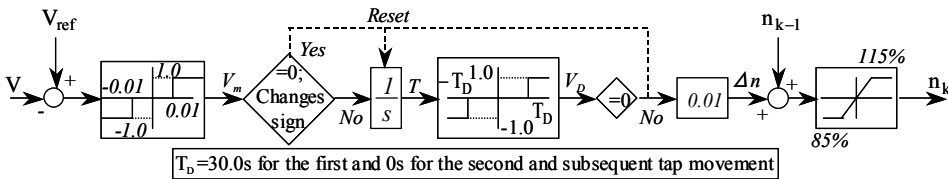


Fig. A4: OLTC control for transformers

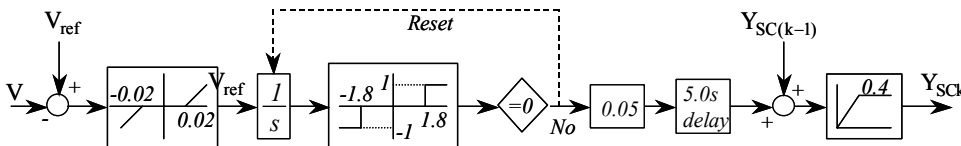


Fig. A5: ACSC control